NJC

PAPER

View Article Online
View Journal

Cite this: DOI: 10.1039/c5nj03002a

Evaluation and synthesis of AZT prodrugs with optimized chemical stabilities: experimental and theoretical analyses†

Sergio R. Ribone,[a] Esteban M. Schenfeld,[b] Marcela Madrid,[c] Adriana B. Pierini*[a] and Mario A. Quevedo*[b]

Received (in Nottingham, UK)
29th October 2015,
Accepted 7th January 2016

DOI: 10.1039/c5nj03002a

www.rsc.org/njc

The design of prodrugs of nucleoside reverse transcriptase inhibitors (NRTIs) constitutes a promising strategy to overcome several suboptimal pharmacotherapeutic properties of these kinds of drugs, among which zidovudine (AZT) is the most studied example. The chemical stability of prodrugs is a critical issue in the context of their pharmacotherapeutic performance since it constitutes a key event in the reconversion of the bioactive NRTIs. In this study, five prodrugs of AZT and lamivudine (3TC) were studied by means of DFT and classical molecular dynamics (MD) strategies in order to model the reaction coordinates involved in their chemical hydrolysis, and extend these conclusions to further structure rationalization of prodrugs. Therefore, the inclusion of explicit water molecules was found to be of great relevance to the mentioned reaction coordinates since it allowed a very good correlation between calculated reaction energy values and the corresponding hydrolysis constants. Based on these findings, three ester based prodrugs of AZT were designed, synthesized and evaluated regarding their chemical stability. These prodrugs exhibited optimized chemical stabilities when compared to the previously reported AZT prodrugs, which may result in an enhanced pharmacotherapeutic performance. In conclusion, the developed theoretical model provides a valuable assistance in the design and development of novel prodrugs of NTRIs with rationalized chemical stabilities.

1. Introduction

The nucleoside reverse transcriptase inhibitors (NRTIs) were among the first family of drugs approved by the Food and Drug Administration (FDA) to treat infection by human immunodeficiency virus type-1 (HIV-1),[1] the etiological agent of the acquired immunodeficiency syndrome (AIDS) in humans. Among the NRTIs, two of the most representative members are zidovudine (AZT, Fig. 1a) and lamivudine (3TC, Fig. 1b).[1]

Both, AZT and 3TC are key components within the combination of anti HIV agents currently used as part of the highly active antiretroviral therapy (HAART)[2] protocols, and as such they have exhibited a vastly demonstrated clinical efficacy. Unfortunately, these drugs have several suboptimal pharmacotherapeutic properties, most of which represent major limitations to their therapeutic use.[3] This situation has motivated intensive efforts to optimize the chemical properties responsible for their clinical performance. Numerous studies have dealt with the optimization of the pharmacokinetic properties of AZT, with much effort focused on prolonging its relatively short plasmatic half-life ($t_{1/2}$ ~1 h).[4] This short $t_{1/2}$ originates by different causes such as: (a) high hepatic first-pass metabolism, with

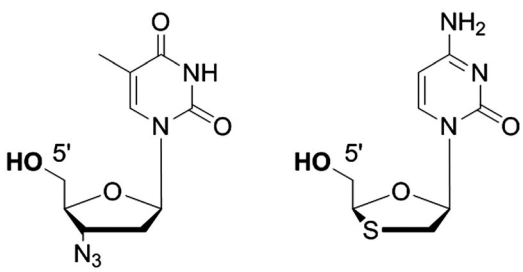

a: AZT b: 3TC

Fig. 1 Molecular structures of AZT and 3TC.

[a] Instituto de Investigaciones en Fisicoquímica de Córdoba (INFIQC, CONICET), Departamento de Química Orgánica, Facultad de Ciencias Químicas, Universidad Nacional de Córdoba, Córdoba, X5000HUA, Argentina. E-mail: adriana@fcq.unc.edu.ar
[b] Unidad de Investigación y Desarrollo en Tecnología Farmacéutica (UNITEFA, CONICET), Departamento de Farmacia, Facultad de Ciencias Químicas, Universidad Nacional de Córdoba, Córdoba, X5000HUA, Argentina. E-mail: alfredoq@fcq.unc.edu.ar; Tel: +54-351-5353865
[c] Pittsburgh Supercomputing Center, Pittsburgh, PA 15213, USA

† Electronic supplementary information (ESI) available. See DOI: 10.1039/c5nj03002a

glucuronidation taking place at its 5′-OH position,[5] and (b) a low fraction bond to human serum albumin (HSA),[6] the main transporter protein in plasma. As a consequence, the intrinsic pharmacokinetic performance of AZT demands the administration of relatively high doses in order to maintain effective antiviral concentrations in plasma,[7] which leads to frequent life-threatening toxic effects.[3] Significant efforts have been made to overcome the mentioned issues by applying different chemical strategies. In particular, the design of prodrugs of NRTIs constitutes a very promising strategy, and has been widely applied to the preparation of prodrugs of AZT that may exhibit enhanced pharmacotherapeutic properties.[8–13] Considering that NRTIs require phosphorylation of the 5′-OH to exhibit anti-HIV activity,[1] many prodrugs have been prepared by derivatization of this position to design inactive compounds that require chemical and/or enzymatic hydrolysis before bioactivity is regained. With this strategy in mind, the possibility of rationalizing and/or predicting the extent of chemical and/or enzymatic reconversion is a keystone for the design of new prodrugs.

During the past decades, several families of AZT and 3TC 5′-OH prodrugs have been reported by different research groups.[8,10,12,13] In line with these efforts, we have developed several 5′-OH derivatized prodrugs of AZT and 3TC, using bioreversible chemical bonds, such as ester, carbonate and carbamate functional groups (Fig. 2).[14–16] Also, the use of linker chains for the design of "double prodrugs" has been an interesting design strategy.[8,10,12,14,17]

As stated before, the chemical stability of the resulting prodrugs represents a critical issue for their pharmacotherapeutic performance since its extent constitutes a key event in the reconversion to the bioactive NRTIs. Previous results obtained at our and other laboratories demonstrated that AZT carbamates are highly resistant to chemical and enzymatic hydrolysis,[18,19] while carbonate and ester based prodrugs exhibit a wide stability range depending on their chemical nature.[20,21] Also, a careful selection of the molecular complement for the design of a double prodrug is required from the beginning because the stability of the chemical bond between the NRTIs and the linker chain may be affected by the added chemical moiety, as demonstrated for a series of AZT prodrugs obtained by our research group by combining AZT oxalic acid ester and several aminoacids.[21] Consequently, the design of 5′-OH prodrugs of NRTIs requires a substantial rationalization of the structural and physicochemical properties underlying both the chemical and enzymatic reconversion processes.

In this work, we studied the structural and energetic details that underlie the chemical hydrolysis of five 5′OH prodrugs of AZT and 3TC previously obtained by our research group, by applying computational quantum mechanics methods to model the corresponding reaction coordinates. Among the studied prodrugs, ester, carbonate and carbamate moieties were included (Fig. 2) in the search for a rational basis correlating the calculated reaction energies with their experimentally determined stabilities. Based on these conclusions, three ester prodrugs of AZT were designed, synthesized and evaluated for their chemical stability.

2. Results and discussion

2.1. Chemical hydrolysis: theoretical studies

The chemical hydrolysis of the studied prodrugs was modeled by simulating the nucleophilic attack of an explicit hydroxyl group on the carbonyl carbon corresponding to the ester, carbonate and carbamate moiety of the 5′-OH prodrugs of AZT and 3TC. These simulations were performed assuming different solvation models. Initial structures of the corresponding compounds were obtained performing multi replicas of simulated annealing molecular dynamics (MD) simulations. In all cases, identical conformations corresponding to the NRTI scaffold were found, in which an anti conformation between the base and the sugar ring was found. This feature is in agreement with previous studies in which the most stable conformer for AZT was obtained applying discrete solvent models and quantum mechanical calculations.[22,23]

2.1.1. Hydrolysis of prodrugs 1–5: solvent as a polarized continuum model (PCM). The first simulation approach involved a solvating environment modeled by PCM.[24] The energy values obtained for the stationary points evaluated under these conditions, as well as the previously reported experimental hydrolysis constants[18,20] are summarized in Table 1. This solvation model suggests that the first transition state (TS1) constitutes the reaction limiting step (ESI,† Fig. S1 and S2). Carbamate prodrugs (**2** and **3**, Table 1) exhibited the highest TS1 energy values among the analyzed prodrugs ($\approx$15 kcal mol^{-1}), which is in agreement

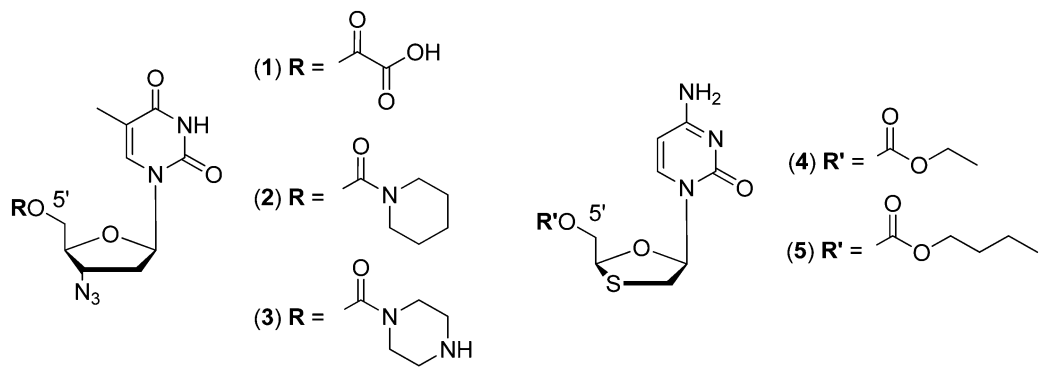

Fig. 2 Molecular structures of AZT and 3TC prodrugs.

Table 1 Energy values (kcal mol^{-1} relative to reactants) of the stationary points corresponding to the hydrolysis reaction coordinates of prodrugs **1–5** (PCM), with their experimentally determined chemical stabilities under neutral and alkaline conditions at 37 °C

	Reaction path stationary points				Chemical stability				
					Neutral conditions		Alkaline conditions		
Prodrug	TS1	INT	TS2	PC	k (h^{-1})	$t_{1/2}$ (h)	k (h^{-1})	$t_{1/2}$ (h)	Ref.
1	5.87	0.99	1.92	−8.91	5.1×10^{-2}	13.6	3.85	0.18	—
2	15.11	7.06	9.28	−3.22	Stable[a]	Stable[a]	6.2×10^{-2}	11.2	18
3	13.91	5.98	7.97	−3.27	Stable[a]	Stable[a]	0.17	4.0	18
4	6.03	−2.19	2.76	−2.73	5.0×10^{-3}	141.5	nd	nd	19
5	5.99	−3.04	0.75	−3.15	1.4×10^{-2}	49.3	nd	nd	19

[a] After 80 h of study; nd: not determined.

with the observed experimental results that demonstrated their high stability at pH 7.4 for at least 80 h.[18] Compound **3** exhibited a slightly lower TS1 energy value compared to that of compound **2**, which is consistent with the lower stability of the former as determined under alkaline conditions (Table 1).[18] When the TS1 energy values obtained for compounds **1**, **4** and **5** were analyzed, no correlation with the experimentally determined values was observed (Table 1), finding almost identical TS1 energy values (≈6 kcal mol^{-1}) for **1**, **4** and **5**. These results show that the application of a PC solvation model is not adequate to describe the hydrolysis reaction path of the studied ester and carbonate prodrugs. This observation suggests that the inclusion of explicit solvent molecules within the reaction coordinate may be required to achieve consistency with the experimental results.[25–28] Previous reports dealing with the hydration properties of AZT have shown the role of explicit water molecules on its physicochemical properties,[22] including its three dimensional structure. Thus, a significant effect of explicit water molecules may also be expected in relation to the chemical stability of NRTI prodrugs.

2.1.2. Hydrolysis of prodrugs 1–5: solvation shell analysis. The involvement of explicit water molecules in the hydrolysis of **1–5** was evaluated by studying the corresponding solvation shells, applying MD simulations. In this way, MD trajectories (50 ns) were obtained under explicit solvent and periodic boundary conditions. From these trajectories, the hydrogen bond interactions between water molecules and oxygen atoms within the ester, carbonate and carbamate scaffolds were monitored by measuring the corresponding radial distribution function (RDF).

Fig. 3 depicts the calculated values of RDF around the carbonyl carbon of prodrugs **1–5**. As can be seen, the carbonyl carbon is always surrounded by a first layer of water molecules located at approximately 3.5 Å from the reactive center, which corresponds to the solvation shell of the adjacent carbonyl oxygen evidenced by the corresponding RDF analysis (ESI,† Fig. S3). In addition, compound **1** was the only one exhibiting a second water layer located at 4.5 Å from the reactive center, which corresponds to the solvation shell of the adjacent ionized carboxylic moiety. This differential behavior among the above mentioned solvent environments surrounding the reactive center in each prodrug strongly suggests that explicit modeling of water molecules as part of the simulated system are required to reach consistency with experimental values.

The structural role of water molecules was further studied by analyzing the substrate-solvent hydrogen bond (HB) network,

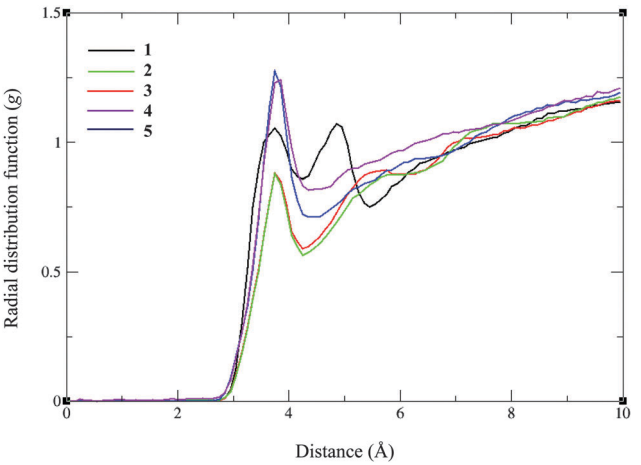

Fig. 3 Radial distribution function (RDF) of water molecules around the carbonyl carbon of prodrugs **1–5**.

with the highest occupied percentages of interaction being quantified. Prodrug **1** displayed three main HB interactions (Fig. 4); each of them showed occupancies of 44.98, 46.27 and 46.30%. These results are in agreement with the solvation shells determined by RDF analyses (Fig. 3 and 4).

Hydrogen bond analyses on both carbamate (Fig. 5a and b) and carbonate prodrugs (Fig. 5c and d) evidenced their capability to establish HB interactions with water molecules through their carbonyl oxygen atom, with occupancy percentages ranging

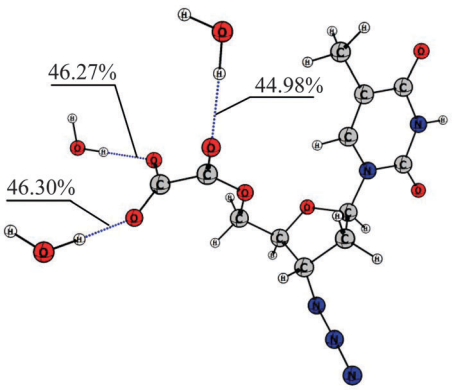

Fig. 4 Water molecule interactions and occupation percentage for prodrug **1** as determined by the hydrogen bond analysis.

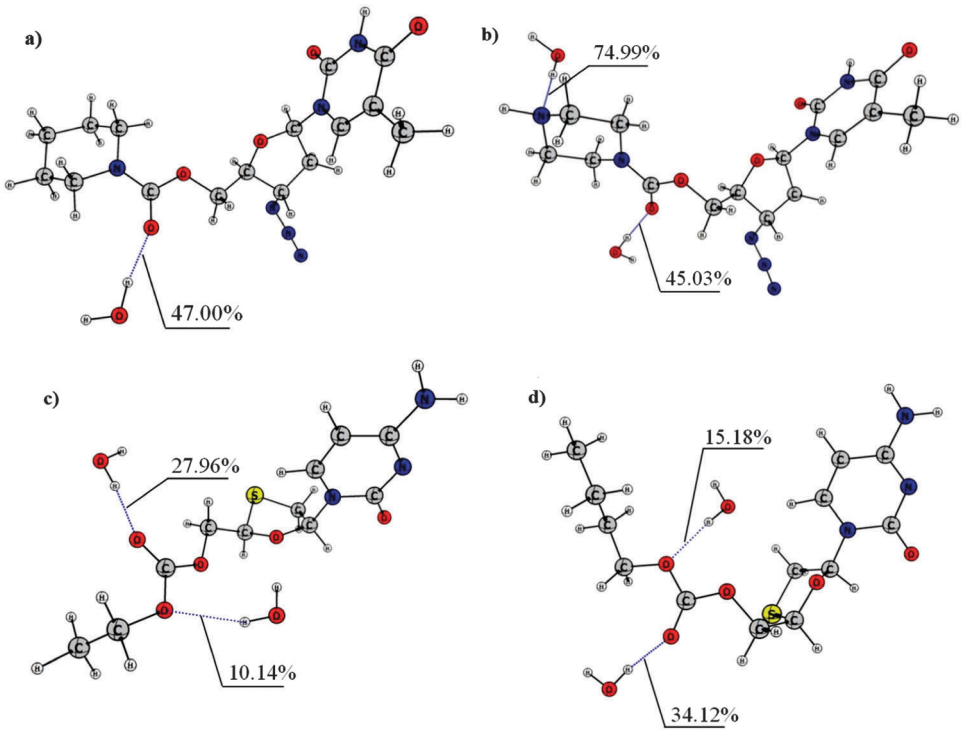

Fig. 5 Hydrogen bond interactions involving water and their occupancy percentage for prodrugs **2**, **3**, **4** and **5** (a–d, respectively).

between 27.96 and 47%. Moreover, compounds **3–5** exhibited a second HB interaction, in which carbamate **3** interacted through the cyclic amine (Fig. 5b), while carbonates **4** and **5** established them through the second oxygen atom of the carbonate group (Fig. 5c and d). As previously commented, RDF and hydrogen bond analyses showed the presence of clustered water molecules surrounding the carbonyl carbon atoms of the studied prodrugs, which indicates their potential involvement in the hydrolysis reaction path. To assess this effect, the corresponding reaction coordinate profiles were studied in the presence of the above mentioned explicit water molecules. Only those solvent molecules establishing an H-bond to the atoms surrounding the reactive center and exhibiting an occupancy percentage higher than 10% were retained for the purpose of reaction coordinates studies with DFT functionals and full geometry optimization.

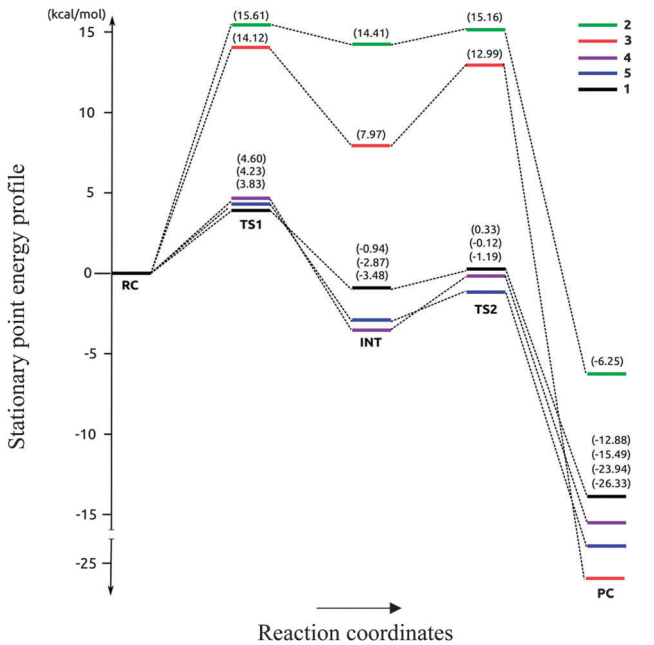

Fig. 6 Energy profile (kcal mol^{-1}) for the simulated hydrolysis stationary points of prodrugs **1–5**, under an explicit water molecule model (EWM).

2.1.3. Hydrolysis of prodrugs 1–5: solvent as explicit water molecules (EWM). Considering the solvation role of explicit water molecules described in Section 2.1.2, the reaction coordinates for the chemical hydrolysis of the studied prodrugs were studied, including these solvent molecules. Also, an additional water molecule was manually added at HB distance and fully optimized to solvate the hydroxyl group. As found under continuum solvent conditions, TS1 stationary points were again identified as the limiting step for the hydrolysis of prodrugs **1–5** (Fig. 6). Consistent with the experimental measurements, carbamates **2** and **3** displayed the highest TS1 energy, with calculated values in the range of 15 kcal mol^{-1}. No significant differences were found between the results obtained under PCM and EWM conditions for the hydrolysis of **2** and **3**, which evidence that the presence of water is not critical to model the hydrolysis of these two prodrugs. On the other hand, ester **1** and carbonates **4** and **5** exhibited considerably diminished TS1 energy values, with slightly different magnitudes among them. This feature is in agreement with their experimental stabilities that showed a significant hydrolysis extent under both neutral and alkaline conditions (Table 1). Also, the most unstable compound was

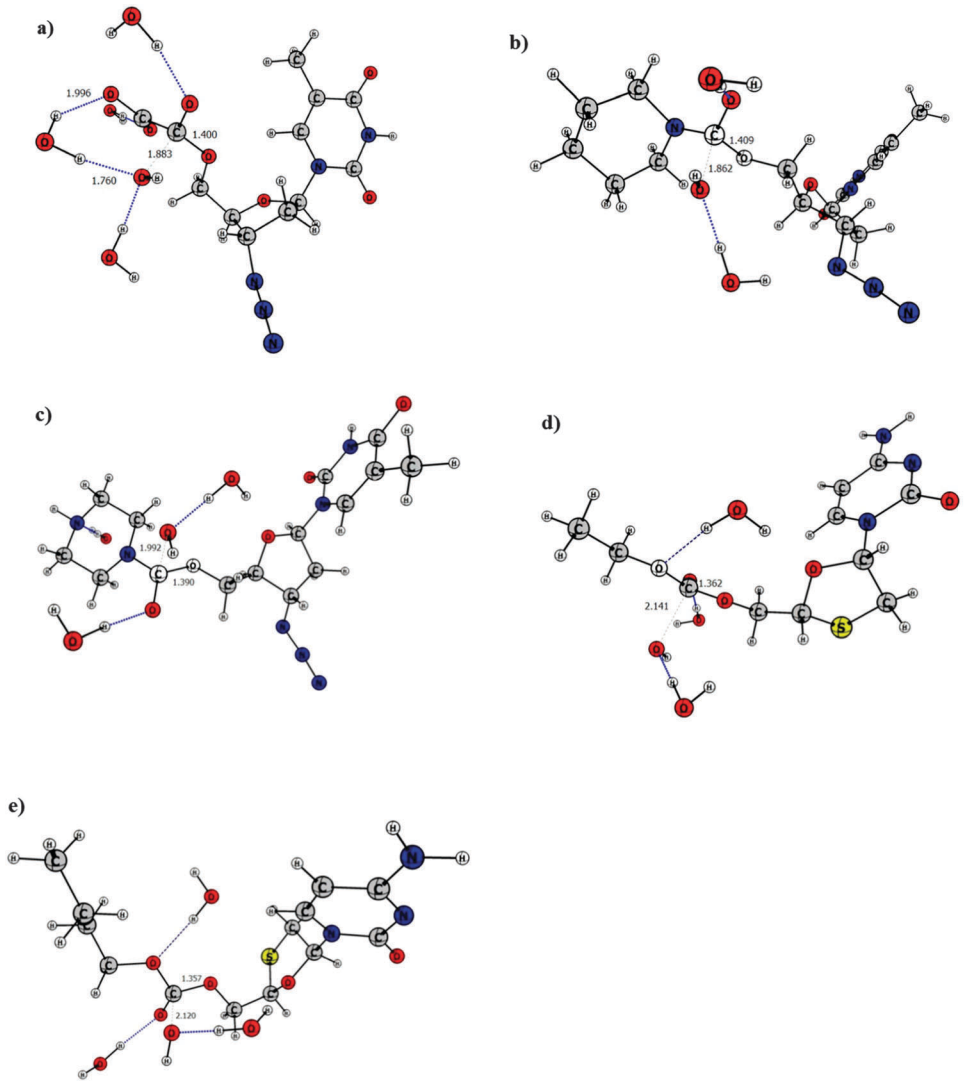

Fig. 7 TS1 geometries in the hydrolysis simulation of (a) ester **1**, (b) carbamate **2**, (c) carbamate **3**, (d) carbonate **4** and (e) carbonate **5** prodrugs, under the EWM model.

the ester based prodrug **1** (TS1: 3.83 kcal mol^{-1}), followed by **5** and **4** (TS1: 4.23 and 4.60 kcal mol^{-1}, respectively). Taking into account this agreement between experimental and theoretical techniques, it is evident that the presence of explicit water molecules plays an important role in the modeling of the hydrolysis reaction coordinates of these prodrugs, particularly of compound **1**.

A detailed analysis of the molecular geometries corresponding to TS1 of prodrug **1** (Fig. 7a) showed a HB mediated stabilization of the attacking hydroxide ion which is exerted by one of the waters solvating the carboxylate group. This event led to a marked decrease in the TS1 stationary point energy when EWM and PCM approaches were compared, which also suggests that the relatively high chemical instability of prodrug **1** may be originated by the spatial proximity between the highly solvated carboxyl group and the carbonyl carbon. In contrast, the absence of intramolecular water molecules capable of exerting an extra solvation on the attacking hydroxide in prodrugs **2–5** (Fig. 7b–e) resulted in an increased chemical stability.

To further study the structural features originating the observed differences between TS1 stationary point energies of carbamates and carbonates, atomic Natural Bond Orbital (NBO) charges and the resulting electrostatic potentials were calculated for the initial conformations of prodrugs **2–5** (Fig. S4–S7, ESI†). These calculations showed slightly higher positive electrostatic potentials and NBO charges on the carbonyl carbons of both carbonate prodrugs compared to those of carbamate derivatives, a feature that would make the former more susceptible to nucleophilic attack by the hydroxyl ion. These findings are in line with the higher values of TS1 and the increased chemical stabilities of both carbamate prodrugs if compared to the studied carbonate derivatives.

2.1.4. Design and evaluation of ester prodrugs with enhanced chemical stability. To further study the above presented hypothesis, three additional ester prodrugs of AZT were designed and evaluated (Fig. 8, compounds **6–8**), in which the ionized carboxyl moieties

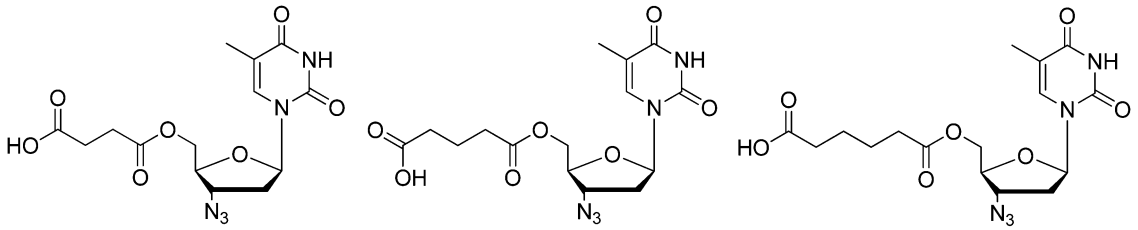

Fig. 8 Molecular structures of the designed AZT prodrugs.

were linked to the carbonyl carbon through methylene spacers. The design criteria aimed to enhance their chemical stabilities by increasing the distance between the ionized group and the reactive center.

Prodrugs **6–8** were subjected to theoretical studies following identical computational protocols as described in Sections 2.1.2 and 2.1.3. From the corresponding molecular dynamic trajectories, the RDF of water molecules around the reactive centers was determined and compared to that of **1** (Fig. 9). In line with the study hypothesis, the second solvation shell observed for **1** at 4.5 Å was not observed for **6**, **7** or **8**.

In the case of **6**, an increased RDF value was observed at about 6 Å, which originates from the spatial interaction between water molecules solvating the prodrug carbonyl carbon (first solvation shell) and water molecules surrounding the carboxylate group. For compounds **7** and **8**, the distance between the carbonyl carbon and the carboxylate group is increased by the presence of additional methylene groups, which in turn hinders such interaction, resulting in the absence of the second solvation shell.

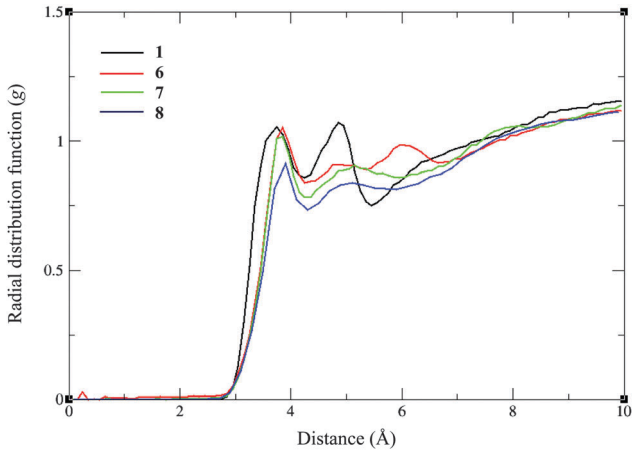

Fig. 9 Radial distribution function (RDF) of water molecules with respect to the carbonyl carbon of prodrugs **1**, **6–8**.

Also, hydrogen bond interaction analyses showed that compounds **6–8** still established three HB interactions with water molecules through the oxygen atoms (Fig. 10). As was the case for compound **1**, interactions were established with the carbonyl oxygen atom (**I**, Fig. 10) and the carboxylic oxygen atoms (**II** and **III**, Fig. 10). The corresponding HB occupancy percentages between explicit water molecules and the carboxylic oxygen atoms (**II** and **III**) ranged between 43 and 48%, resulting in similar values to that calculated for **1** (46%, Fig. 4), while interactions established with the carbonyl oxygen (**I**) ranged between 35.46 and 38.73%, resulting in slightly lower values compared to that calculated for **1** (45%, Fig. 4).

The above results are in line with the hypothesis stating that these three ester prodrugs may exhibit an enhanced chemical stability compared to **1**. Therefore, the corresponding reaction coordinates including explicit water molecules were further investigated (Fig. 11). Once again the formation of TS1, with calculated stationary point energy values of 6.31, 6.20 and 5.34 kcal mol^{-1}, for **6**, **7** and **8**, respectively, was the limiting step of the reaction (Fig. 11, Table 2). These TS1 energy values were higher than that calculated for **1** (3.83 kcal mol^{-1}), a feature that is originated in the absence of the intramolecular water molecules that exert the extra solvation on the attacking hydroxide due to the higher distance between the carboxyl group and the carbonyl carbon (ESI,† Fig. S8).

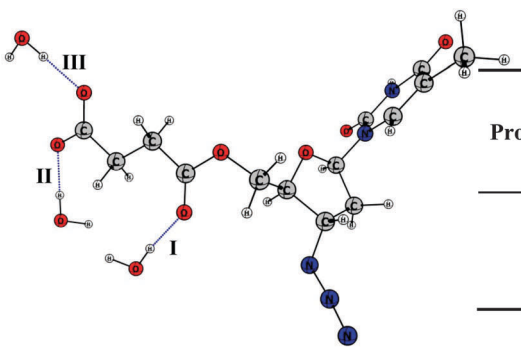

Prodrug	Hydrogen bond acceptor atom occupied percentage		
	I	II	III
6	36.50	43.28	42.97
7	38.73	48.51	48.46
8	35.46	46.84	45.62

Fig. 10 Water molecule interaction and occupancy percentage for prodrugs **6–8** from the hydrogen bond analysis.

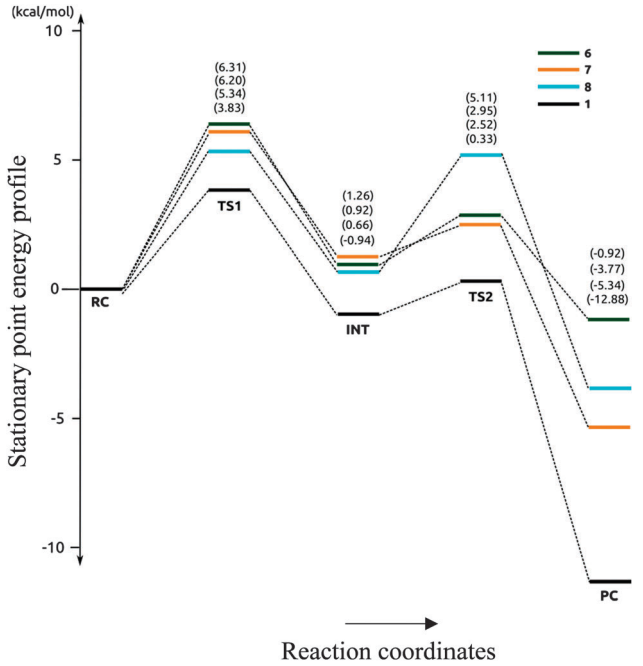

Fig. 11 Energy profile (kcal mol^{-1}) for the simulated hydrolysis stationary points of **1**, and **6–8**, under the explicit water molecule model (EWM).

2.2. Synthesis and chemical stability evaluation of 6, 7 and 8

To support the conclusions derived from the computational studies, prodrugs **6**, **7** and **8** were synthesized and their chemical stability under acidic (pH 2), neutral (pH 7.4) and alkaline (pH 10) conditions was experimentally determined.

The synthesis of compounds **6–8** was conducted by condensation of AZT with the corresponding dicarboxylic acids (succinic, glutaric and adipic acid, respectively) in the presence of *N*′,*N*′-dicyclohexylcarbodiimide (DCC) and 4-dimethylaminopyridine (DMAP), using dichloromethane (DCM) as solvent (Scheme 1). The reaction progressed at room temperature for 24–48 h.

In this synthetic procedure, two molecules of the corresponding organic diacid reacted *in situ* to give an anhydride intermediate which occurred with the intervention of DCC.[29] After this initial step, AZT reacted through its 5′-OH moiety with the anhydride, resulting in the desired product that was subsequently isolated and purified. This methodology is a convenient procedure to prepare these prodrugs if compared to previous reports.[12,17]

Finally, the chemical stability of prodrugs **1**, **6–8** was assayed under acid, neutral and alkaline conditions for 48 h, to obtain the corresponding concentration *vs.* time profiles (ESI,† Fig. S9, S10 and Tables S1 and S2). All the prodrugs displayed a high stability under acidic conditions (pH 2) for 48 h, thus AZT was not quantified in the reaction media (data not included). In addition, **6–8** also showed a marked chemical stability at pH 7.4, while compound **1** suffered hydrolysis under these experimental conditions, with a calculated $t_{1/2}$ of 12.8 h. As expected, when alkaline conditions (pH 10) were evaluated, all the prodrugs exhibited higher chemical hydrolysis reaction rates, with $t_{1/2}$ values ranging between 0.18 and 11.85 h. Once again, prodrugs **6–8** exhibited considerably higher stabilities than that of **1**.

These experimental results are in agreement with the presented computational studies, which demonstrated that the proximity between the carbonyl carbon (reactive center) and the highly solvated carboxylic moiety constitutes a critical structural feature driving the chemical stability of this family of ester based AZT prodrugs.

Table 2 Energy values (kcal mol^{-1} relative to reactants) of the stationary points corresponding to the hydrolysis reaction coordinates of prodrugs **1**, **6–8** (EWM), with their experimentally chemical stability under neutral (pH 7.4) and alkaline (pH 10) conditions at 37 °C

	Reaction path stationary points				Chemical stability			
					pH 7.4		pH 10	
Prodrugs	TS1	INT	TS2	PC	k (h^{-1})	$t_{1/2}$ (h)	k (h^{-1})	$t_{1/2}$ (h)
1	3.83	−0.94	0.33	−12.88	5.4×10^{-2}	12.8	3.91 ± 0.05	0.18
6	6.31	0.92	2.95	−0.92	Stable[a]	Stable[a]	$5.9 \times 10^{-2} \pm 2.9 \times 10^{-2}$	11.85
7	6.20	1.26	2.52	−5.34	Stable[a]	Stable[a]	0.110 ± 0.007	6.31
8	5.34	0.66	5.11	−3.77	Stable[a]	Stable[a]	0.110 ± 0.004	6.29

[a] No AZT detected after 48 h of study.

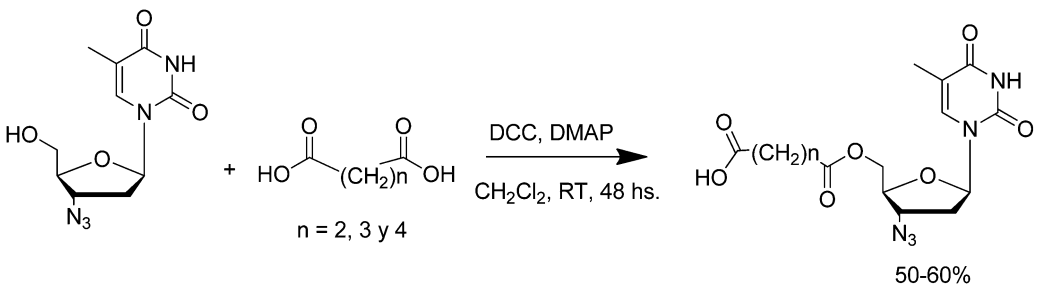

Scheme 1 Synthetic procedure involved in the obtaining of prodrugs **6–8**.

3. Conclusions

In this work, the design of novel AZT prodrugs with optimized chemical stabilities was conducted by applying quantum chemical computational studies, using different molecular modeling strategies to rationalize and further enhance the hydrolytic susceptibility of the previously reported prodrugs. The radial distribution function of water molecules around the carbonyl carbon atom of ester, carbonate and carbamate prodrugs highlighted the importance of solvent molecules in assisting their chemical hydrolysis.

The simulated reaction coordinates corresponding to these hydrolysis studies required explicit modeling of water molecules, and demonstrated that their effect was necessary to reach consistency between the first transition state stationary point energy values (rate-limiting step of the reaction) and the experimental chemical stability observations. Therefore, the energetic assistance of solvent molecules to the attacking hydroxyl ion was identified to be responsible for the high chemical instability of prodrug **1**.

In light of the structural features identified, three ester based prodrugs of AZT were designed and synthesized employing a convenient method. Both theoretical and experimental chemical stability studies on these additional prodrugs evidenced their higher stability with respect to the previous AZT ester prodrug **1**, with calculated $t_{1/2}$ values being compatible with the desired reconversion rates of AZT from the corresponding prodrug. It is noteworthy that prodrugs exhibiting a very high stability, such as those reported for carbamates **2** and **3** are not desired because of the low regeneration rates of the bioactive lead compound.

In overall terms, it can be stated that the present work of research may constitute a useful aid for the design and development of novel ester based prodrugs of nucleoside reverse transcriptase inhibitors with optimized chemical stabilities. Also, the inclusion of additional chemical scaffolds by derivatization of the acidic moiety of prodrugs **6–8** may represent an interesting strategy to obtain "double prodrugs". In this case, the chemical stability prediction methodology presented in this work may support medicinal chemists in selecting adequate chemical scaffolds that confer modulated chemical stabilities.

4. Computational and experimental details

4.1. Computational methods

4.1.1. Initial conformation of prodrugs. Initial geometries of the simulated molecules were obtained by means of molecular dynamics techniques applying simulated annealing (SA)[30] procedures. To perform these studies, the GAFF force field[31] was used to parameterize the prodrugs, which were further solvated in a TIP3P water box and simulated under periodic boundary conditions. Standard molecular dynamics procedures were applied, including two minimization phases (solvent and whole system) and a heating stage (from 0 to 300° K) followed by an equilibration (1 ns, 300° K) phase. The resulting systems constituted the starting conformations to perform SA schemes, in which the systems were heated from 300 to 1200° K, maintained during 1 000 000 steps, and then gently cooled down to 0° K in 100° K ramps of 100 000 steps each. The whole simulation scheme involved 10 ns of trajectory, including 5 000 000 steps. SA protocols were repeated 10 times. When clustering analyses of the final structures resulting from each iteration were performed, reproducible conformations were obtained and thus the final prodrug structures were considered as the lowest energy conformations. A time step of 2 fs was applied in all MD procedures. The Amber14 software package was used to perform these studies.[32]

4.1.2. Chemical hydrolysis simulations. The conformations obtained by MD were further subjected to full geometry optimization at DFT levels by applying the B3LYP/6-311+G* basis set.[33,34] In all cases, the effect of the solvent was assessed using the Tomasi's polarized continuum model (PCM)[24,35,36] as implemented in Gaussian09 software.[37] Transition states (TS) and the corresponding intermediates were identified by a scan of distinguished reaction coordinate with full optimization of the remaining geometric parameters. The characterization of stationary points was performed by Hessian matrix calculations, obtaining positive eigenvalues for minimum states (reactive, intermediate and product) and one negative eigenvalue for each TS.[38] The energy values reported for all species included zero-point corrections which were calculated by applying the standard statistical-mechanics relationship for an ideal gas.[39]

4.1.3. Radial distribution function (RDF) and hydrogen bond (HB) analyses. The contribution of explicit water molecules to the hydrolysis of the studied prodrugs was preliminarily explored by means of RDF and HB analyses. Starting from the optimized molecular structure (refer to Section 4.1.2), and applying the above mentioned MD procedure (refer to Section 4.1.1), each prodrug was submitted to further MD simulation for 50 ns to obtain extended trajectories on which quantitative RDF and HB analyses were performed by including water molecules within a 10 Å radius around the reactive center. Both analyses were carried out using the cpptraj[40] module of Amber14.[32] Water molecules exhibiting the highest interaction percentage were selected and kept explicit during the reaction coordinate simulations, while the rest of the solvent system was stripped. The resulting systems were re-optimized at DFT levels, with the minimized systems being used to initiate the hydrolysis reaction coordinate study (Section 4.1.2). The hydroxide ion was also solvated with an additional water molecule and fully optimized prior to the obtaining of the reaction coordinates.

4.2. Experimental methods

4.2.1. Chemicals and reagents. All chemical reagents were obtained from commercial sources (Sigma-Aldrich and Fluka) and were used without further purification. AZT was generously provided by Filaxis Laboratories (Buenos Aires, Argentina). All solvents were reagent or HPLC grade. Chemical reactions were monitored by thin layer chromatography (TLC) on precoated silica gel plates with fluorescent indicator UV_{254} (Macherey-Nagel); spots were visualized with UV light. ^{1}H NMR and ^{13}C NMR spectra were recorded on a 400 MHz Bruker spectrometer. Chemical shifts are reported in parts per million (ppm).

4.2.2. General procedure for the synthesis of 1, 6–8. Compound **1** was synthesized as previously reported.[14] For the synthesis of compounds **6–8**, 331 mg of *N*′,*N*′-dicyclohexylcarbodiimide (1.5 mmol, 1.5 eq.), 15 mg of 4-dimethylaminopyridine (0.12 mmol, 0.12 eq.) and the corresponding dicarboxylic acid (2.5 mmol, 2.5 eq.) were dissolved in 5 ml of anhydrous dichloromethane and kept under stirring for 15 minutes in an ice bath, after which the reaction continued at room temperature for 24 h. In a second stage, AZT (267 mg, 1.0 mmol, 1 eq.) was added to the reaction media and further stirred for 48 h at room temperature. The resulting mixture was filtered and afterwards extracted with 5 M HCl (3 × 10 ml). The organic phase was dried over Na_2SO_4 and evaporated under vacuum to obtain the product as white solid foam. Yields of the purified prodrugs were always between 50–60%, and were confirmed by means of HPLC analyses (ESI,† Fig. S11).

4.2.2.1. 3′-Acido-3′-deoxy-5′-O-succinylthymidine acid (6)[12]. This prodrug was obtained using succinic acid as dicarboxylic acid, with the corresponding product being obtained in yields of 58% (216 mg), mp: 59–60 °C. ^{1}H NMR (400 MHz, Acetone, TMS): δ (ppm) = 1.87 (d, 3H, J = 1.2 Hz, 7-H), 2.52 (dm, 2H, J = 26.2 Hz, 2′-H), 2.69 (m, 4H, J = 25.2, 2″-H and 3″-H), 4.11 (q, 1H, J = 13.4 Hz, 4′-H), 4.40 (dd, 2H, J = 16.6Hz, 5′-H), 4.51 (dt, 1H, J = 18.0 Hz, 3′-H), 6.24 (t, 1H, J = 13.1 Hz, 1′-H), 7.54 (d, 1H, J = 1.2 Hz, 6-H). ^{13}C NMR (400 MHz, Acetone, TMS): δ (ppm) = 11.59 (C7), 28.30 (C3″), 28.36 (C2″), 36.53 (C2′), 60.67 (C3′), 63.27 (C5′), 81.55 (C4′), 84,50 (C1′), 110.36 (C5), 135.73 (C6), 150.36 (C2), 163.46 (C4), 171.92 (C1″), 172.98 (C4″). HRMS (ESI) *m/z* calcd for $C_{14}H_{16}N_5O_7^-$ $[M - H]^-$: 366.1055, found 366.1101.

4.2.2.2. 3′-Acido-3′-deoxy-5′-O-glutarylthymidine acid (7). This prodrug was obtained using glutaric acid as dicarboxylic acid, with the corresponding product being obtained in yields of 60% (229 mg), mp: 56–57 °C. ^{1}H NMR (400 MHz, Acetone, TMS): δ (ppm) = 1.87 (d, 3H, J = 1.2 Hz, 7-H), 1.93 (q, 2H, J = 14.72 Hz, 3″-H), 2.41 (t, 2H, J = 7.24 Hz, 2′-H), 2.53 (m, 4H, J = 71.4, 2″-H and 4″-H), 4.13 (q, 1H, J = 13.9 Hz, C*H*-4′), 4.39 (dq, 2H, J = 16.8 Hz, 5′-H), 4.53 (dt, 1H, J = 18.0 Hz, 3′-H), 6.23 (t, 1H, J = 13.1 Hz, 1′-H), 7.51 (d, 1H, J = 1.2 Hz, 6-H). ^{13}C NMR (400 MHz, Acetone, TMS): δ (ppm) = 11.61 (C7), 20.00 (C3″), 32.23 (C4″), 32.69 (C2″), 36.51 (C2′), 60.90 (C3′), 63.31 (C5′), 81.50 (C4′), 84,70 (C1′), 110.30 (C5), 135.70 (C6), 150.31 (C2), 163.35 (C4), 172.22 (C1″), 173.34 (C5″). HRMS (ESI) *m/z* calcd for $C_{15}H_{18}N_5O_7^-$ $[M - H]^-$: 380.1212, found 380.1244.

4.2.2.3. 3′-Acido-3′-deoxy-5′-O-adipylthymidine acid (8). This prodrug was obtained using adipic acid as dicarboxylic acid, with the corresponding product being obtained in yields of 52% (204 mg), mp: 48–49 °C. ^{1}H NMR (400 MHz, Acetone, TMS): δ (ppm) = 1.68 (m, 4H, J = 37.7 Hz, 3″-H and 4″-H), 1.87 (d, 3H, J = 1.3 Hz, 7-H), 2.34 (m, 2H, J = 28.1 Hz, 2′-H), 2.53 (m, 4H, J = 28.1 Hz, 2″-H and 5″-H), 4.12 (q, 1H, J = 13.9 Hz, 4′-H), 4.40 (dq, 2H, J = 16.8 Hz, 5′-H), 4.52 (dt, 1H, J = 18.1 Hz, 3′-H), 6.22 (t, 1H, J = 13.1 Hz, 1′-H), 7.52 (d, 1H, J = 1.2 Hz, 6-H). ^{13}C NMR (400 MHz, Acetone, TMS): δ (ppm) = 11.64 (C7), 24.15 (C3″ and C4″), 32.94 (C5″), 33.31 (C6″), 36.52 (C2′), 60.90 (C3′), 63.27 (C5′), 81.52 (C4′), 84,74 (C1′), 110.30 (C5), 135.81 (C6), 150.36 (C2), 163.50 (C4), 172.43 (C1″), 173.78 (C6″). HRMS (ESI) *m/z* calcd for $C_{16}H_{20}N_5O_7^-$ $[M - H]^-$: 394.1368, found 394.1415.

4.2.3. Determination of chemical stabilities

4.2.3.1. Preparation of stock solutions and the assay procedure. Stock solutions of **6–8** (2.6×10^{-3} M) were prepared on the day of assay in an acetonitrile: methanol (80 : 20) mixture. Chemical stabilities were measured at different pH values by preparing the corresponding phosphate buffers (100 mM): (a) pH 7.4 (8.63 mg ml^{-1} Na_2HPO_4; 4.70 mg ml^{-1} NaH_2PO_4) and (b) pH 10 (8.63 mg ml^{-1} Na_2HPO_4), all of which were prepared in milli-Q water as indicated. Working solutions (25 ml, 1.4×10^{-4} M) were obtained by conveniently diluting each stock solution in the corresponding phosphate buffer.

To carry out the stability assay, working solutions were fractionated in 12 aliquots (2 ml each) and incubated at 37° until sampling was conducted. For studies performed at pH 7.4, aliquots were sampled at convenient time intervals for 48 h, while for assays performed at pH 10, sampling was performed for 24 h. All aliquots were subjected to convenient preparation procedures prior to quantitative analysis.

4.2.3.2. Sample preparation procedure. To process samples for HPLC analysis, a solid phase extraction (SPE) methodology was developed and fully validated using Strata-X Phenomenex® SPE cartridges. The procedure involved five analytical steps: (a) cartridges were preconditioned by sequentially adding 2.0 ml of methanol, followed by (b) an equilibration step of 2.0 ml of pH 2 (100 mM) phosphate buffer. A selected internal standard IS (compounds **6**, **7** and **8**, depending on the analytes quantified) was added to the sample, homogenized and (c) applied to the preconditioned cartridge at a flow rate of 1 drop per s, and dried under vacuum for 1 min. The (d) elution step was performed with 1 ml of HPLC grade ACN, which was afterwards (e) evaporated to dryness under a N_2 stream at 40 °C, and stored at −20 °C. On the day of analysis, samples were resuspended in 100 μl of methanol, and subjected to HPLC analysis.

4.2.3.3. HPLC apparatus and analyses. The HPLC analysis was carried out in an Agilent Series 1100 apparatus equipped with an autosampler module, thermostatic column compartments and an Agilent Multiple Wavelength Detector (MWD®) set at 267 nm. Instrumental control and chromatographic data acquisition were performed using the Agilent ChemStation (Rev. B.03.01) software. Chromatographic separations were performed using a Phenomenex Synergy Fusion® C_{18} analytical column (4.0 × 250 mm, 5 μm particle size) equipped with a Phenomenex Security Guard Fusion® RP (4.0 × 30 mm) guard column. The mobile phase consisted of a pH 2.0 phosphate buffer (0.1 mM): methanol: tetrahydrofuran (44 : 54 : 2) mixture, at a flow rate of 1 ml min^{-1}. The analytical and guard columns were thermostated at 40 °C, and then 5 μl of sample solution was injected in each chromatographic run.

Acknowledgements

The authors gratefully acknowledge financial support from the Secretaria de Ciencia y Técnica of the Universidad Nacional de

Córdoba (SECYT-UNC), the Consejo Nacional de Investigaciones Científicas y Técnicas (CONICET) and the Agencia Nacional de Promoción Científica y Técnica (ANPCyT), Argentina. This research was supported in part by the National Science Foundation through XSEDE resources provided by the Pittsburgh Supercomputing Center (TG-MCB070064). Authors also acknowledge the GPGPU Computing Group from the Facultad de Matemática, Astronomía y Física (FAMAF), Universidad Nacional de Córdoba, Argentina, for providing access to computing resources. Sergio R. Ribone also acknowledges postdoctoral fellowship from CONICET.

Notes and references

1 E. De Clercq, *Int. J. Antimicrob. Agents*, 2009, **33**, 307–320.
2 E. De Clercq, *Curr. Opin. Pharmacol.*, 2010, **10**, 507–515.
3 G. D'Andrea, F. Brisdelli and A. Bozzi, *Curr. Clin. Pharmacol.*, 2008, **3**, 20–37.
4 L. L. Bruton, *Goodman and Gilman's The Pharmacological Basis of Therapeutics*, McGraw-Hill, New York, 2011.
5 K. H. P. Moore, R. H. Raasch, K. L. R. Brouwer, K. Opheim, S. H. Cheeseman, E. Eyster, S. M. Lemon and C. M. Van der Horst, *Antimicrob. Agents Chemother.*, 1995, **39**, 2732–2737.
6 M. A. Quevedo, S. R. Ribone, G. N. Moroni and M. C. Briñón, *Bioorg. Med. Chem.*, 2008, **16**, 2779–2790.
7 D. E. Bastiaans, T. R. Cressey, H. Vromans and D. M. Burger, *Expert Opin. Drug Metab. Toxicol.*, 2014, **10**, 1019–1037.
8 W. Li, Y. Chang, P. Zhan, N. Zhang, X. Liu, C. Pannecouque and E. De Clercq, *ChemMedChem*, 2010, **5**, 1893–1898.
9 Y. Zhang, Y. Gao, X. Wen and H. Ma, *Asian J. Pharm. Sci.*, 2014, **9**, 65–74.
10 A. Dalpiaz, G. Paganetto, B. Pavan, M. Fogagnolo, A. Medici, S. Beggiato and D. Perrone, *Mol. Pharmaceutics*, 2012, **9**, 957–968.
11 G. Giacalone, H. Hillaireau and E. Fattal, *Eur. J. Pharm. Sci.*, 2015, **75**, 40–53.
12 S. Wannachaiyasit, P. Chanvorachote and U. Nimmannit, *AAPS PharmSciTech*, 2008, **9**, 840–850.
13 P. N. Solyev, A. V. Shipitsin, I. L. Karpenko, D. N. Nosik, L. B. Kalnina, S. N. Kochetkov, M. K. Kukhanova and M. V. Jasko, *Chem. Biol. Drug Des.*, 2012, **80**, 947–952.
14 G. N. Moroni, P. M. Bogdanov and M. C. Briñón, *Nucleosides, Nucleotides Nucleic Acids*, 2002, **21**, 231–241.
15 S. Ravetti, M. S. Gualdesi, J. S. Trinchero-Hernández, G. Turk and M. C. Briñón, *Bioorg. Med. Chem.*, 2009, **17**, 6407–6413.
16 M. A. Raviolo, J. S. Trinchero-Hernández, G. Turk and M. C. Briñón, *J. Braz. Chem. Soc.*, 2009, **20**, 1870–1877.
17 A. Neeraj, M. J. N. Chandrasekar, U. V. S. Sara and A. Rohini, *Drug Delivery*, 2011, **18**, 272–280.
18 M. A. Raviolo and M. C. Briñón, *Sci. Pharm.*, 2011, **79**, 479–491.
19 P. N. Solyev, A. V. Shipitsin, I. L. Karpenko, D. N. Nosik, L. B. Kalnina, S. N. Kochetkov, M. K. Kukhanova and M. V. Jasko, *Chem. Biol. Drug Des.*, 2012, **80**, 947–952.
20 M. S. Gualdesi, S. Ravetti, M. A. Raviolo and M. C. Briñón, *Drug Dev. Ind. Pharm.*, 2014, **40**, 1246–1252.
21 M. A. Raviolo, J. Esteve-Romero and M. C. Briñón, *J. Chromatogr. A*, 2011, **1218**, 2540–2545.
22 M. Alcolea Palafox and J. Talaya, *J. Phys. Chem. B*, 2010, **114**, 15199–15211.
23 M. A. Palafox, *Phys. Chem. Chem. Phys.*, 2014, **16**, 24763–24783.
24 J. Tomasi, B. Mennucci and R. Cammi, *Chem. Rev.*, 2005, **105**, 2999–3093.
25 Y. Q. Fang and E. N. Jacobsen, *J. Am. Chem. Soc.*, 2008, **130**, 5660–5661.
26 R. B. Sunoj and M. Anand, *Phys. Chem. Chem. Phys.*, 2012, **14**, 12715–12736.
27 Y. Xia, Y. Liang, Y. Chen, M. Wang, L. Jiao, F. Huang, S. Liu, Y. Li and Z. X. Yu, *J. Am. Chem. Soc.*, 2007, **129**, 3470–3471.
28 G. O. Andrés, A. B. Pierini and R. H. De Rossi, *J. Org. Chem.*, 2006, **71**, 7650–7656.
29 B. Neises and W. Steglich, *Angew. Chem., Int. Ed. Engl.*, 1978, **17**, 522–524.
30 S. Kirkpatrick, C. D. Gelatt Jr and M. P. Vecchi, *Science*, 1983, **220**, 671–680.
31 J. Wang, R. M. Wolf, J. W. Caldwell, P. A. Kollman and D. A. Case, *J. Comput. Chem.*, 2004, **25**, 1157–1174.
32 R. Salomon-Ferrer, D. A. Case and R. C. Walker, *Wiley Interdiscip. Rev.: Comput. Mol. Sci.*, 2013, **3**, 198–210.
33 A. D. Becke, *Phys. Rev. A: At., Mol., Opt. Phys.*, 1988, **38**, 3098–3100.
34 C. Lee, W. Yang and R. G. Parr, *Phys. Rev. B: Condens. Matter Mater. Phys.*, 1988, **37**, 785–789.
35 R. Improta, V. Barone, G. Scalmani and M. J. Frisch, *J. Chem. Phys.*, 2006, **125**, 000.
36 R. Improta, G. Scalmani, M. J. Frisch and V. Barone, *J. Chem. Phys.*, 2007, **127**, 000.
37 M. J. Frisch, G. W. Trucks, H. B. Schlegel, G. E. Scuseria, M. A. Robb, J. R. Cheeseman, G. Scalmani, V. Barone, B. Mennucci, G. A. Petersson, H. Nakatsuji, M. Caricato, X. Li, H. P. Hratchian, A. F. Izmaylov, J. Bloino, G. Zheng, J. L. Sonnenberg, M. Hada, M. Ehara, K. Toyota, R. Fukuda, J. Hasegawa, M. Ishida, T. Nakajima, Y. Honda, O. Kitao, H. Nakai, T. Vreven, J. A. Montgomery, Jr., J. E. Peralta, F. Ogliaro, M. Bearpark, J. J. Heyd, E. Brothers, K. N. Kudin, V. N. Staroverov, R. Kobayashi, J. Normand, K. Raghavachari, A. Rendell, J. C. Burant, S. S. Iyengar, J. Tomasi, M. Cossi, N. Rega, J. M. Millam, M. Klene, J. E. Knox, J. B. Cross, V. Bakken, C. Adamo, J. Jaramillo, R. Gomperts, R. E. Stratmann, O. Yazyev, A. J. Austin, R. Cammi, C. Pomelli, J. W. Ochterski, R. L. Martin, K. Morokuma, V. G. Zakrzewski, G. A. Voth, P. Salvador, J. J. Dannenberg, S. Dapprich, A. D. Daniels, Ö. Farkas, J. B. Foresman, J. V. Ortiz, J. Cioslowski and D. J. Fox, *Gaussian 09, Revision E.01*, Gaussian, Inc., Wallingford CT, 2009.
38 J. W. McIver Jr and A. Komornicki, *J. Am. Chem. Soc.*, 1972, **94**, 2625–2633.
39 P. Atkins and J. de Paula, *Physical Chemistry*, Oxford University Press, New York, 8th edn, 2006.
40 D. R. Roe and T. E. Cheatham, *J. Chem. Theory Comput.*, 2013, **9**, 3084–3095.

